Ocean-Land-Atmosphere Research
A SCIENCE PARTNER JOURNAL

RESEARCH ARTICLE

High-Frequency Observations of Plankton and Particle Abundance from a Cabled Observatory Off Japan

Hidekatsu Yamazaki[1,2,3*], Silvana B. Penninck[4], Gabriel Freitas[3], Leandro T. De-La-Cruz[4], Marika Takeuchi[5], Mamoru Tanaka[6], and Rubens M. Lopes[4]

[1]School of Marine Science, Sun Yat-sen University, Zhuhai, China. [2]Marine Biophysicist Unit, Okinawa Institution of Science and Technology, Okinawa, Japan. [3]School of Marine Resources and Environment, Tokyo University of Marine Science and Technology, Tokyo, Japan. [4]Department of Biological Oceanography, Oceanographic Institute, University of São Paulo, São Paulo, Brazil. [5]Ocean BioGeosciences, National Oceanography Centre, Southampton, UK. [6]Department of Civil Engineering, Tokyo University of Science, Tokyo, Japan.

*Address correspondence to: hide@kaiyodai.ac.jp

Citation: Yamazaki H, Penninck SB, Freitas G, De-La-Cruz LT, Takeuchi M, Tanaka M, Lopes RM. High-Frequency Observations of Plankton and Particle Abundance from a Cabled Observatory Off Japan. *Ocean-Land-Atmos. Res.* 2026;5:Article 0132. https://doi.org/10.34133/olar.0132

Submitted 14 February 2025
Revised 14 January 2026
Accepted 22 January 2026
Published 6 March 2026

In August 2014, a cabled observatory was deployed off Oshima Island, south of Tokyo, Japan, and operated until September 2018, yielding a 4-year dataset of oceanographic properties and plankton abundance at a fixed location. This study highlights the variability of key physical and biological parameters observed during 2 distinct periods of this time series. Data were collected using a suite of instruments such as thermistor chains, acoustic Doppler velocimeter (ADV), acoustic Doppler current profiler (ADCP), conductivity, temperature, depth (CTD), turbidity and fluorescence sensor, photosynthetically active radiation (PAR) sensor, wave height gauge, and CPICS (a plankton imaging system). Based on these observations, the kinetic energy dissipation rate was estimated over time and its correlation with plankton abundance, aggregate abundance, and plankton diversity was examined. The results demonstrated that temperature fluctuations followed a −5/3 power-law spectrum across the observed frequency range, consistent with turbulence theory. Plankton diversity, measured using the Shannon index, exhibited a power-law spectrum with a slope of −1 (f^{-1}) for harmonic components exceeding 4 h in duration, characterized by a daily peak corresponding to zooplankton diel vertical migration. Long-term measurements of turbulence remain scarce but are crucial for understanding seasonal to interannual variability in plankton and particle dynamics. These findings underscore the importance of ocean mixing in regulating size distribution and abundance, offering insights into the interplay between physical and biological processes in coastal ecosystems.

Introduction

Marine plankton are fundamental to the functioning of marine ecosystems, because they drive primary productivity, regulate fishery yields, and play a pivotal role in the biological carbon pump, a critical mechanism for greenhouse gas sequestration [1,2]. Physical processes, such as turbulence and mixing, affect plankton distribution and aggregate formation [3,4,5,6]. These aggregates contribute considerably to carbon fluxes by serving as food for zooplankton and higher trophic levels while enhancing vertical carbon transport [7].

Phytoplankton growth and biomass are regulated by climate-induced changes in ocean structure, including rising upper ocean temperatures, increased stratification, and reduced vertical mixing [8]. Turbulent mixing is modulated by tidal cycles, seasonal wind variations, internal waves, and eddy activities [9,10,11]. Over time scales from days to years, local wind patterns and stratification strongly influence the turbulence intensity in the mixed layer and subsurface waters [12,13]. Long-term turbulence observations are critical for understanding the distributions of key oceanic properties, such as dissolved gases and heat, offering insights into the ocean's response to climate change [14]. Turbulence fluctuations considerably affect plankton communities by enhancing nutrient availability [15,16], altering phytoplankton behavior [17], increasing predator–prey interactions [18], and modulating spatial distribution [19,20,21]. Despite its importance for quantifying seasonal, annual, and long-term mixing processes, high-frequency turbulence observations spanning weeks to months remain scarce.

Time-series data are essential for understanding the spatial and temporal dynamics of plankton abundance. However, many existing time series rely on discrete sampling methods, such as bottle or net collection, followed by microscopic analysis [22,23,24] or remote sensing techniques using pigment

analysis [25]. These traditional approaches often lack the resolution to capture fine-scale temporal variations in the water column, resulting in substantial errors in abundance estimates [26,27,28]. Advances in underwater imaging systems have addressed these limitations by enabling frequent sampling and facilitating the study of fine-scale and long-term biophysical processes [29,30,31]. Imaging systems are now widely used to investigate biophysical interactions and assess biomass and size spectra in water column [32,33,34,35]. Oceanographic moorings equipped with imaging systems enable high-frequency acquisition of spatial and temporal plankton data, enabling detailed analysis of plankton dynamics [36,37,38].

Although imaging-based high-frequency plankton time series exist, they predominantly focus on small-sized organisms such as phytoplankton and microzooplankton [39,40], leaving larger plankton and aggregates underrepresented. This study investigated the relationships among aggregates, plankton abundance, diversity, and microscale physical properties, including turbulence intensity, using data obtained from a cabled observatory in the coastal waters of Oshima Island, Japan [21,41,42]. The analysis focused on two 4-month segments from a 4-year dataset (August 2014 to September 2018) encompassing key oceanographic and biological variables recorded by environmental sensors and a plankton imaging system (CPICS) mounted on a cabled observatory.

Methods

Study area and data acquisition

The study was conducted in the coastal waters surrounding Oshima Island, approximately 100 km south of Tokyo Bay (Fig. 1A). This volcanic island is strongly influenced by the Kuroshio western boundary current and tidally generated internal waves. A cabled observatory system, the Oshima Coastal Environmental data Acquisition Network System (OCEANS;

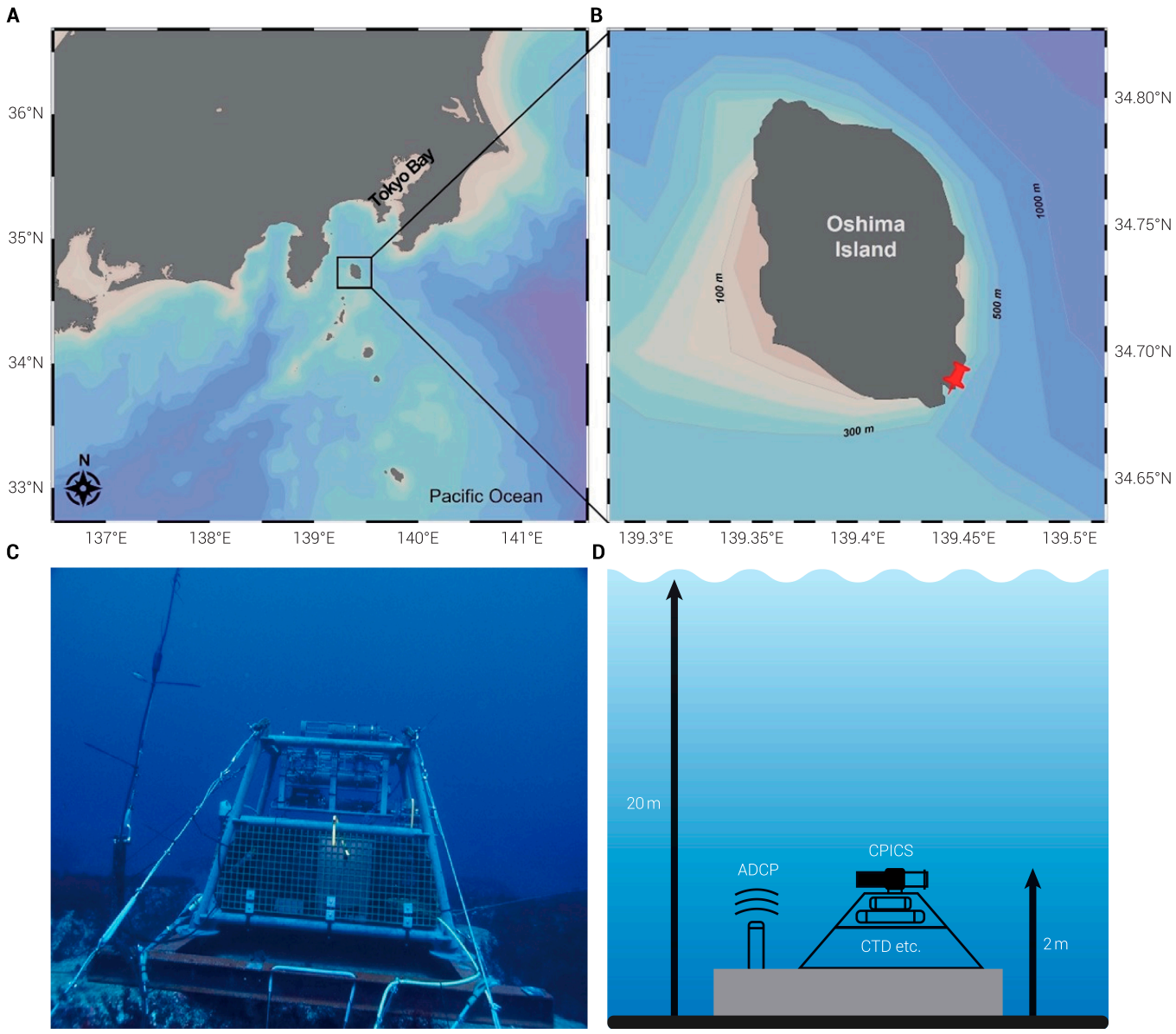

Fig. 1. (A) Map of the study region and (B) the location of the OCEANS observatory at Habu Port (red pin), in the coastal area of Oshima Island. (C) In situ view of the Cabled observatory Oshima Coastal Environmental data Acquisition Network System (OCEANS). (D) Schematic drawing of the CPICS and oceanographic sensors on the OCEANS platform (objects and depths are not to scale).

[21,41,42]), was deployed at a depth of 20 m in Habu Port (34°40′–48′N, 139°21′–28′E; Fig. 1B) to collect physical and biological data. Despite being located within the breakwater, hydrographic conditions closely resembled those outside. The observation area was primarily affected by tidal forcing. Masunaga et al. [43] identified trapped diurnal internal Kelvin waves around Oshima Island using the 3-dimensional Stanford Unstructured Nonhydrostatic Terrain-following Adaptive Navier–Stokes Simulator (SUNTANS). Thermistor chain data from OCEANS confirmed the presence of these predicted Kelvin waves.

The OCEANS observatory operated from 2014 to 2018, providing high-resolution observations. For this study, 2 time-series datasets were selected for analysis.

- TS1: October 2014 to January 2015 (2014/2015)
- TS2: October 2015 to January 2016 (2015/2016)

We selected equal time intervals to examine seasonal and interannual variability in physical and biological parameters, ensuring a large number of observations while maintaining dataset manageable for image processing and automatic classification of plankton taxa.

Environmental data (Table 1) were collected using a suite of instruments installed on the OCEANS platform (Fig. 1C and D) designed to measure key physical and biological parameters. A conductivity, temperature, depth (CTD) (ACTW-CAR, ACLW2-CAR, ALW-RS; JFE Advantech Co. Ltd., Hyogo, Japan) recorded the temperature, conductivity, chlorophyll-a fluorescence, turbidity, and photosynthetically active radiation (PAR). An acoustic Doppler current profiler (ADCP; Aquadopp Profiler 400 kHz; Nortek AS) was used to measure current velocities, whereas an acoustic Doppler velocimeter (ADV; Vector; Nortek AS) was used to measure turbulence. The wave heights were estimated using a pressure sensor (AWH-RS; JFE Advantech Co. Ltd., Hyogo, Japan).

Plankton imaging data were obtained using the Continuous Plankton Imaging and Classification Sensor (CPICS; [44]). The CPICS is a high-resolution imaging instrument designed for the in situ capture and classification of plankton and particles in aquatic environments. Using a darkfield illumination, the system enhances visibility of fine structural details, enabling detection of particles as small as 50 μm, depending on the instrument's configuration. During deployment, CPICS operated continuously with a field of view measuring 11 mm × 15 mm × 2 mm and captured images at a frequency of 3 Hz. This configuration allowed sampling of 35.6 l of seawater per hour, equivalent to approximately 0.85 m^3 per day. The instrument produces high-resolution frames with dimensions of 2,750 × 2,200 pixels, delivering detailed morphological and textural data suitable for automated classification of objects exceeding 150 μm, the minimum size for reliable identification based on depth of field positioning. Quantitative analysis primarily targeted larger zooplankton and particles, although microphytoplankton and heterotrophic protists were also recorded.

Table 1. List of sensors mounted on the cabled observatory system OCEANS

Sensor	Parameters	Sample rate
Physical		
CT sensor	Temperature, conductivity	1 Hz
T-string	Temperature	1 Hz
ADCP	Current	60 s
ADV	Turbulence	8 Hz
PAR sensor	PAR	1 Hz
Pressure sensor	Pressure, wave height	1 Hz
Biological		
CPICS	Plankton images	3 Hz
Chlorophyll/turbidity sensor	Chlorophyll fluorescence, turbidity	1 Hz

Plankton imaging data and initial processing

Approximately 1.9 million in situ color dark-field images were captured for the durations of TS1 and TS2 deployments. These RGB images were first converted to grayscale and then transformed into a binary format to facilitate analysis using computer vision tools described by Penninck et al. [45] and Penninck and Lopes [46], which require binary input, using the following procedure: Formally, let I_g be a grayscale image and I_b be the binary image computed from I_g, the value of I_b for pixel p is defined as

$$I_b(p) = 1, \text{if } I_g(p) < t; \text{otherwise: } 0 \quad (1)$$

The threshold (t) was estimated from the histogram "h" of image I_g as follows:

$$t = \text{mode}(h) - 2 \times \text{std}(h) \quad (2)$$

Statistical functions such as "mode" and "standard deviation" were applied to define an appropriate value of t. To avoid dealing with noised pixels, the image I_g was smoothed by the application of a Gaussian kernel of size 5 × 5 pixels. The binary image was then computed from the processed version I_g and refined by removing the smallest connected components, filling holes, and connecting adjacent components. This procedure was performed using morphological operators [47,48].

Feature extraction and automatic classification

Descriptors were computed using I_g. In this study, 3 different approaches were applied to extract features from plankton images, with the computation of (a) 55 different morphological features, such as major axis, area, perimeter, and solidity; (b) 10 textural features computed from the histogram of the local binary patterns [49,50]; and (c) 10 textural features obtained from the co-occurrence matrix as described in [51]. A complete list of features is provided in the Supplementary Materials. These features have been extensively employed in machine learning studies dealing with plankton images [52,53,54,55]. Each image I_g was thus represented as a 75-element numerical feature array. The major axis was used as a proxy to estimate plankton and particle size classes.

For image classification, let X be a space of features arrays where $x_i \in X$ is the array containing the features associated to

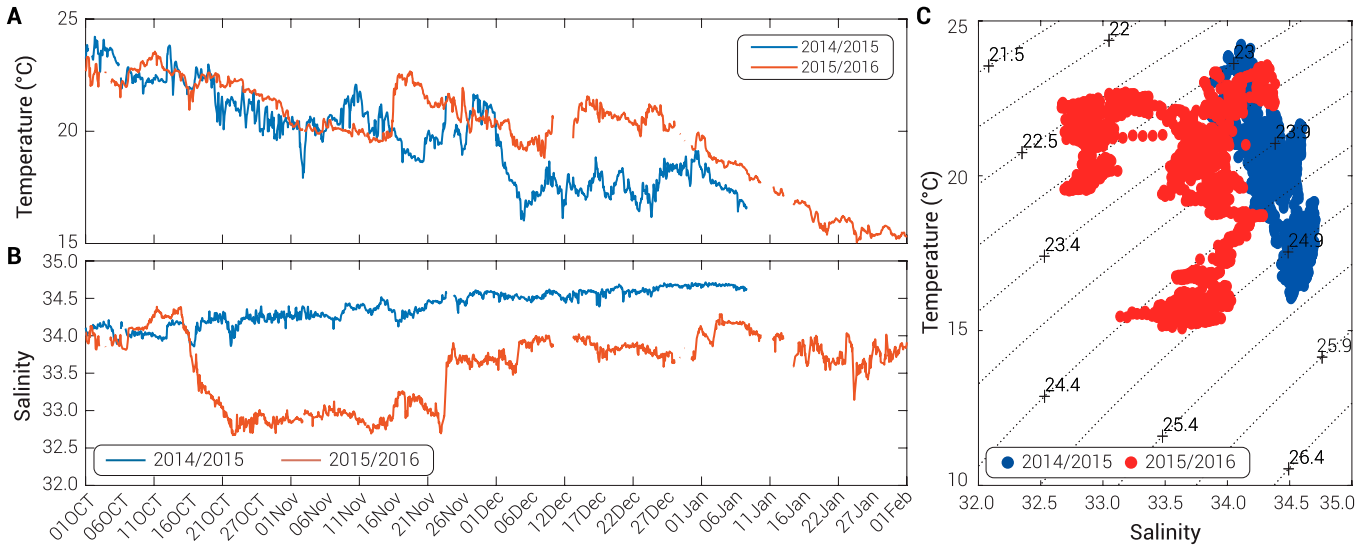

Fig. 2. Time series of (A) temperature (°C) and (B) salinity for the periods from October 2014 to January 2015 (blue line) and October 2015 to January 2016 (orange line). (C) TS diagram for the periods from October 2014 to January 2015 (blue dots) and October 2015 to January 2016 (red dots).

the i-th image of our plankton image dataset. Also, let Y be the space of labels where $y_i \in Y$ is the manual label associated with the i-th image. A typical procedure for a task of supervised classification is divided into 3 phases: (a) create an input dataset of pairs (x_i, y_i); (b) define a classification function $f: X -> Y$; (c) train the function f to adjust the parameters of the classifier model to yield predictions.

In this study, function f was defined using the Random Forest (RF) algorithm [56]. To train the function, 90% of the data were applied, and 10% were used to validate the model. This splitting process was performed by maintaining the proportions of all classes and allowing for the creation of an RF classifier. Finally, the RF classifier was used to predict classes from images belonging to the 2 time-series segments, TS1 and TS2, departing from an initial training set containing a subset of 31,000 manually validated images collected between August 2014 and October 2014. Subsequently, plankton experts manually validated the predicted results.

Shannon diversity index estimation

The Shannon diversity index (H′) was used to estimate high-level diversity for each hourly data [57]:

$$H' = -\sum \frac{N_i}{N} \ln\left(\frac{N_i}{N}\right) \quad (3)$$

where N_i is the number of individuals [regions of interest (ROIs)] sampled for taxon (or particle) i and N is the total number of individuals (ROIs) sampled. In addition to plankton taxa, the nonliving particles included in these calculations were aggregates categorized into 2 classes: aggregate-compact (opaque, solid aggregates), aggregate-amorphous (semi-transparent aggregates), and fecal pellets.

Multivariate analysis

To examine the linear relationships between biological variables (zooplankton, phytoplankton, and particle aggregates) and environmental conditions (temperature, salinity, PAR, chlorophyll-a fluorescence, turbidity, suspended mineral particles, significant wave height, and turbulence), redundancy analysis (RDA) was applied to the entire dataset, which helped in identification of environmental factors that were most strongly associated with variations in biological descriptors. To evaluate the statistical significance of the RDA axes, an analysis of variance (ANOVA) was subsequently performed. All statistical analyses were conducted using R software (version 3.6.3) and the vegan package [58].

Table 2. List of plankton and nonliving particles acquired from the automatic image classification and subsequent manual validation for TS1 and TS2 image samples collected by the CPICS on the OCEANS platform, Oshima Island, Japan.

Metazoan plankton	Phytoplankton and heterotrophic protists	Nonliving particles
Calanoida	*Eucampia*	Aggregates
Cyclopoida	*Rhizosolenia*	Fecal pellets
Harpacticoida	*Chaetoceros*	Mineral (lithogenic) particles
Monstrilloida	Other centric diatoms	Bubbles
Mysida	Benthic (pennate) diatoms	
Amphipoda	*Trichodesmium*	
Isopoda	*Noctiluca scintillans*	
Cumacea	*Tripos*	
Ostracoda	Other dinoflagellates	
Decapoda larvae	*Aulosphaera trigonopa*	
Cirripedia larvae	Other rhizarians	
Other crustaceans		
Polychaeta larvae		
Hydromedusae		
Chaetognatha		
Appendicularia		
Fish eggs		
Fish larvae		

Results

Hydrographic data

The hydrographic conditions observed during TS1 (2014/2015) and TS2 (2015/2016) exhibited clear differences in temperature and salinity. The average temperature was 19.7 °C during TS1, increasing to 20.8 °C in TS2. Salinity showed a decreasing trend, with an average of 34.4 during TS1 and 33.7 during TS2 (Fig. 2).

The temperature time series for both periods displayed similar patterns, characterized by a gradual decline over the respective observation periods. However, salinity during TS2 showed a marked decrease after 2015 October 16. These hydrographic changes are further illustrated in a temperature–salinity (TS) diagram, which highlights distinct water masses. TS1 reflected conditions typical of open-ocean waters influenced by the Kuroshio, whereas TS2 exhibited characteristics of coastal waters, likely influenced by the input of low-salinity waters from Tokyo Bay.

Plankton and particle composition and temporal variability

As expected based on the CPICS image resolution, the collected images mainly captured large metazooplankton and aggregates, followed by an abundance of diatoms, dinoflagellates, and rhizarians, as well as fecal pellets and mineral particles. In total, 33 taxa were detected (Table 2). Representative images of various objects captured by CPICS are presented in Fig. 3, which illustrates the diversity of plankton and particles observed during the study.

Particle counts during both periods were dominated by aggregates, making up 77% of the total images in TS1 and 73% in TS2 (Fig. 4A and B). Zooplankton were the second most abundant group, comprising 10% of the total images in TS1 and increasing to 22% in TS2. Phytoplankton contributed a smaller proportion, representing 6% and 3% of the total images in TS1 and TS2, respectively.

The relative abundances of the major zooplankton and phytoplankton taxa showed notable differences between the observation windows (Fig. 4C and D). Diatoms were the dominant component of TS1, accounting for 45% of the total counts. However, their proportion decreased considerably to 21% in TS2. Copepods displayed the opposite trend, increasing from 15% of the total counts in TS1 to 53% in TS2.

Time-series analysis of copepod and aggregate abundances, along with their respective size fractions, revealed distinct patterns between the 2 periods (Fig. 5). In TS1, copepods

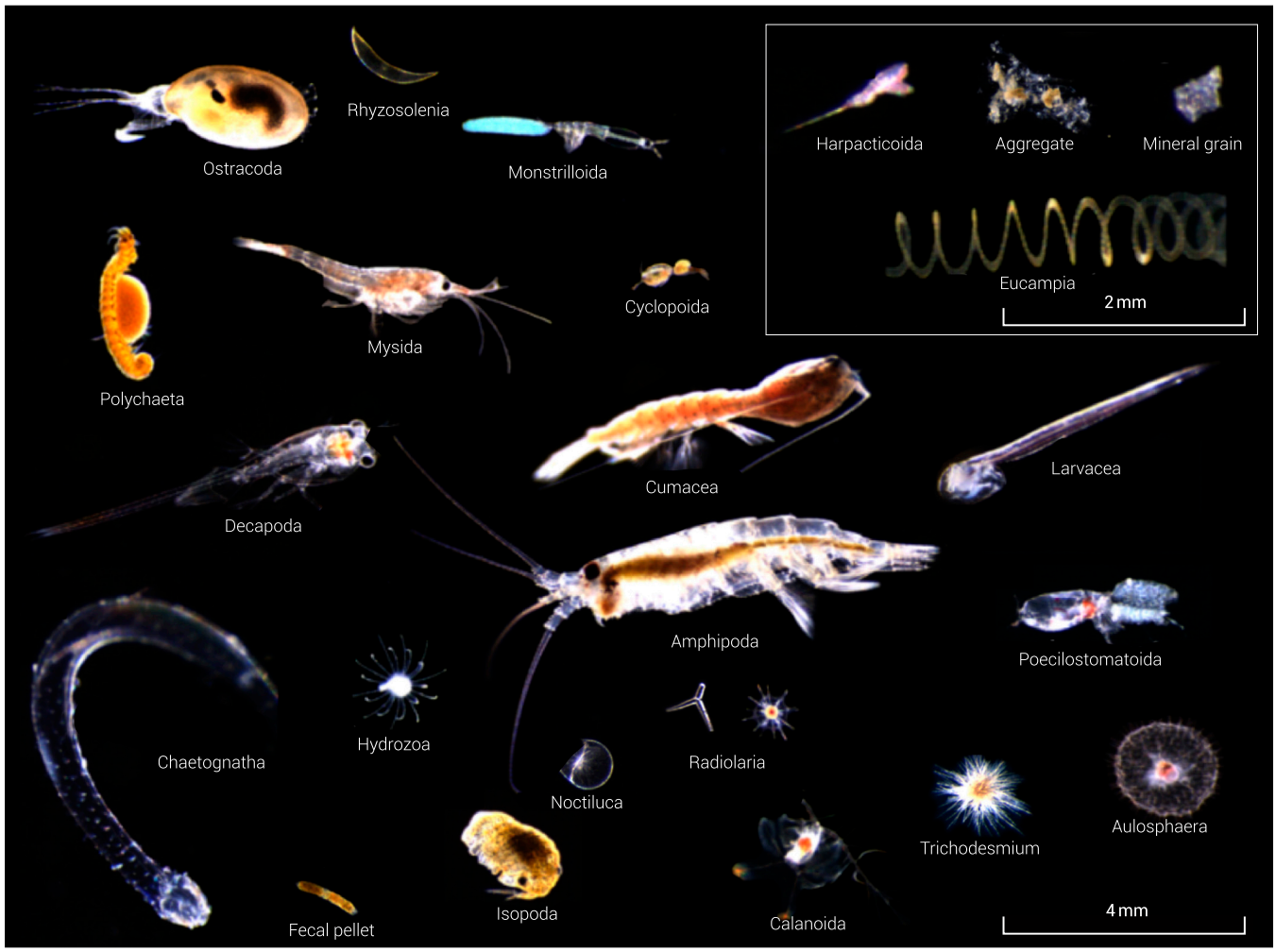

Fig. 3. Color images of different plankton and particle classes observed with the CPICS instrument during the TS1 and TS2 deployments on the OCEANS platform, Oshima Island, Japan.

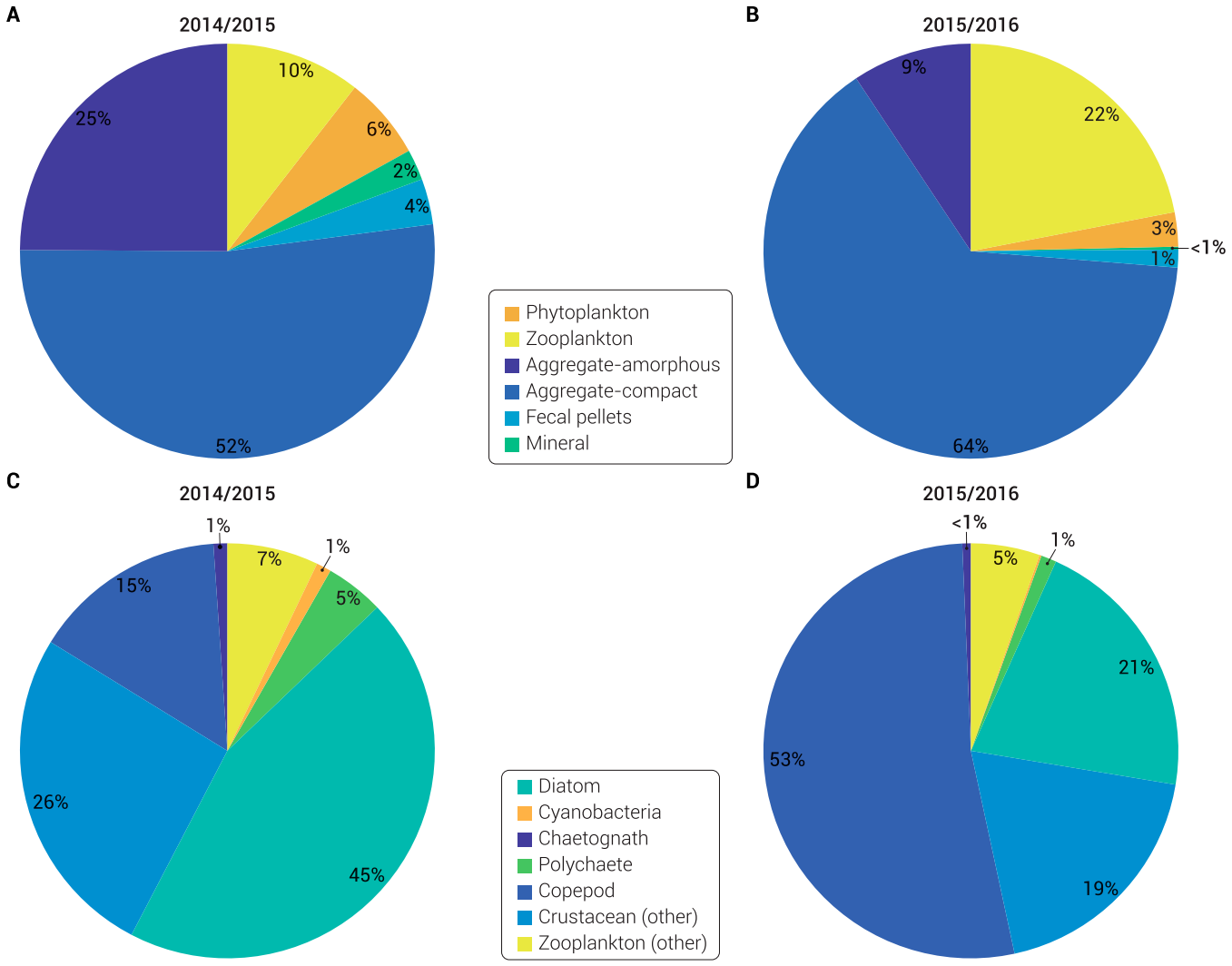

Fig. 4. (A and B) Relative abundances of major particle classes (phytoplankton, zooplankton, amorphous aggregates, compact aggregates, fecal pellets, and minerals) for the time series from October 2014 to January 2015 (TS1) and from October 2015 to January 2016 (TS2). (C and D) Relative abundances of the major phytoplankton (diatoms and cyanobacteria) and zooplankton taxa [chaetognaths, polychaetes, copepods, crustaceans (other), and other zooplankton taxa] for the same time intervals (TS1 and TS2).

predominantly ranged in size from 300 to 1,200 μm, while aggregates were concentrated in the 300- to 600-μm size range. TS2, however, showed a shift toward smaller copepods and aggregates, with sizes below 300 μm becoming more prominent.

Temporal patterns in total copepod abundance peaked in November 2014 and November 2015, both of which coincided with an increased proportion of larger particles. Aggregate abundance reached its highest levels in late October and early November 2014, dominated by smaller particles (<300 μm). There was a marked rise in the proportion of aggregates larger than 300 μm in November 2015, further emphasizing the distinct size distribution trends between the 2 periods.

The abundance of aggregates exhibited substantial temporal variability, with peaks often aligned with increases in turbulence levels (ε), particularly during TS1 (Fig. 6A). In TS1, the occurrence of phytoplankton particles increased toward the end of October 2014 and the beginning of November 2014, coinciding with an increase in aggregate abundance. In contrast, the zooplankton particle counts showed little variation during this period. During TS2, however, the zooplankton abundance increased in early November 2015, whereas the phytoplankton abundance increased in January 2016 (Fig. 6B).

Typhoons were recorded throughout both observation periods. The event of 2014 October 14 to 16 (Fig. 6A) resulted in spikes in the turbulence levels and occasional gaps in the turbulence data, accompanied by maxima in the resuspended mineral particle concentrations. Mineral particles were not observed at the same intensity in other typhoons during any time segment.

During the TS1 period, 3 major storm events were recorded (Fig. 7A), which were characterized by substantially elevated wave heights (Fig. 7B). These storm events were associated with an increase in aggregate abundance (Fig. 7C), from all size classes (Fig. 7D).

Shannon diversity index

The Shannon diversity index was estimated from hourly data, and the time series showed both short-term fluctuations and long-term trends for TS1 and TS2 (Fig. 8A and B). For both

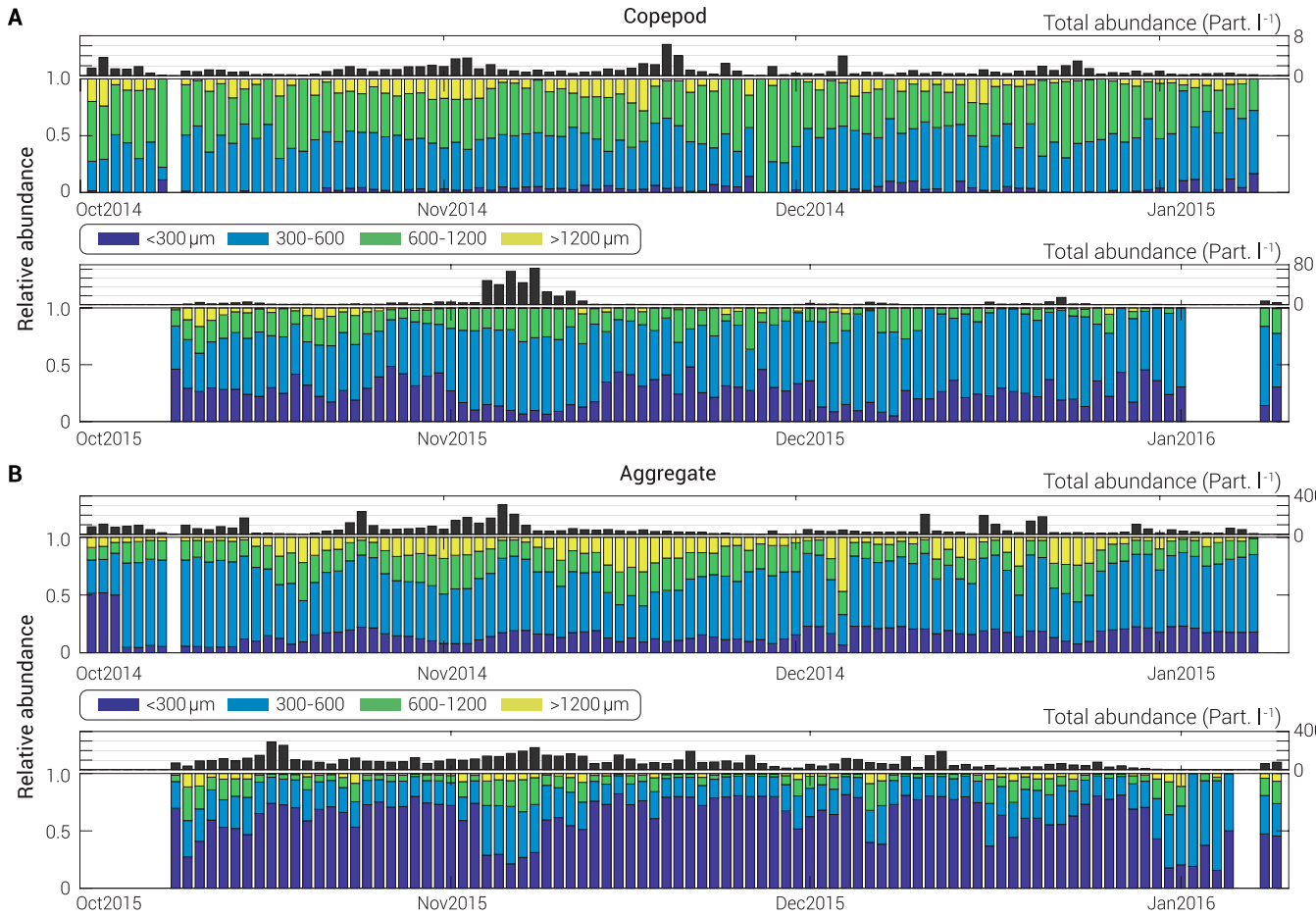

Fig. 5. Time series of daily averages of total (black bar graphs) and relative abundance (colored bar graphs) of (A) copepod size classes and (B) aggregate (amorphous + compact) size classes for both time intervals analyzed in this study, TS1 and TS2 (October 2014 to January 2015 and October 2015 to January 2016).

periods, the long-term trends were negative, with statistical analysis confirming the significance of the slopes and indicating a seasonal decline in diversity as the transition from autumn to winter progressed. Higher diversity values were recorded in October 2015, followed by a sharp decline in November 2015 (Fig. 8B). These fluctuations in diversity mirrored the temporal variability in turbulence data (Fig. 6), suggesting a potential link between physical mixing processes and shifts in planktonic community composition.

Time series analysis

The power spectrum density (PSD) analysis of the temperature time series (Fig. 9A) revealed a consistent −5/3 slope across both datasets, indicating turbulent energy cascades typical of oceanic systems [59]. In contrast, the PSD analysis of the hourly aggregate abundance showed a −5/3 slope at frequencies above the daily cycle. Longer timescales exhibited a −1 slope, commonly referred to as a pink-noise spectrum, which is characteristic of biological systems (Fig. 9B).

PSD analysis of the Shannon diversity index revealed a −1 slope up to a 4-h cycle, with a clear daily peak observed in both datasets. However, for periods shorter than 4 h, the spectrum shifts to a white-noise pattern, indicating a loss of temporal autocorrelation at shorter timescales (Fig. 9C).

Multivariate analysis

RDA revealed that axes 1 and 2 together explained 90% of the total variance, with RDA1 accounting for 68% and RDA2 contributing 22% (Fig. 10). The influence of explanatory variables on response variables was highly significant (ANOVA, $F = 11.5$, $P = 0.001$).

The RDA biplots (Fig. 10) show a clear separation between the 2 sampling periods. TS1 was characterized by higher significant wave height (WH), salinity, and PAR values, whereas TS2 was associated with elevated abundances of phytoplankton, aggregates, and zooplankton. These results indicate that variability in aggregate abundance was strongly influenced by turbulence intensity (ε). Additionally, zooplankton abundance was positively correlated with turbidity and chlorophyll-a fluorescence, suggesting that trophic interactions play an important role in shaping zooplankton dynamics.

Discussion

Research into physical–biological coupling in the ocean is heavily dependent on available technology and sampling methodologies, with long-term and high-frequency measurements remaining rare. High-resolution environmental monitoring and digital imaging at coastal sites in Japan revealed that

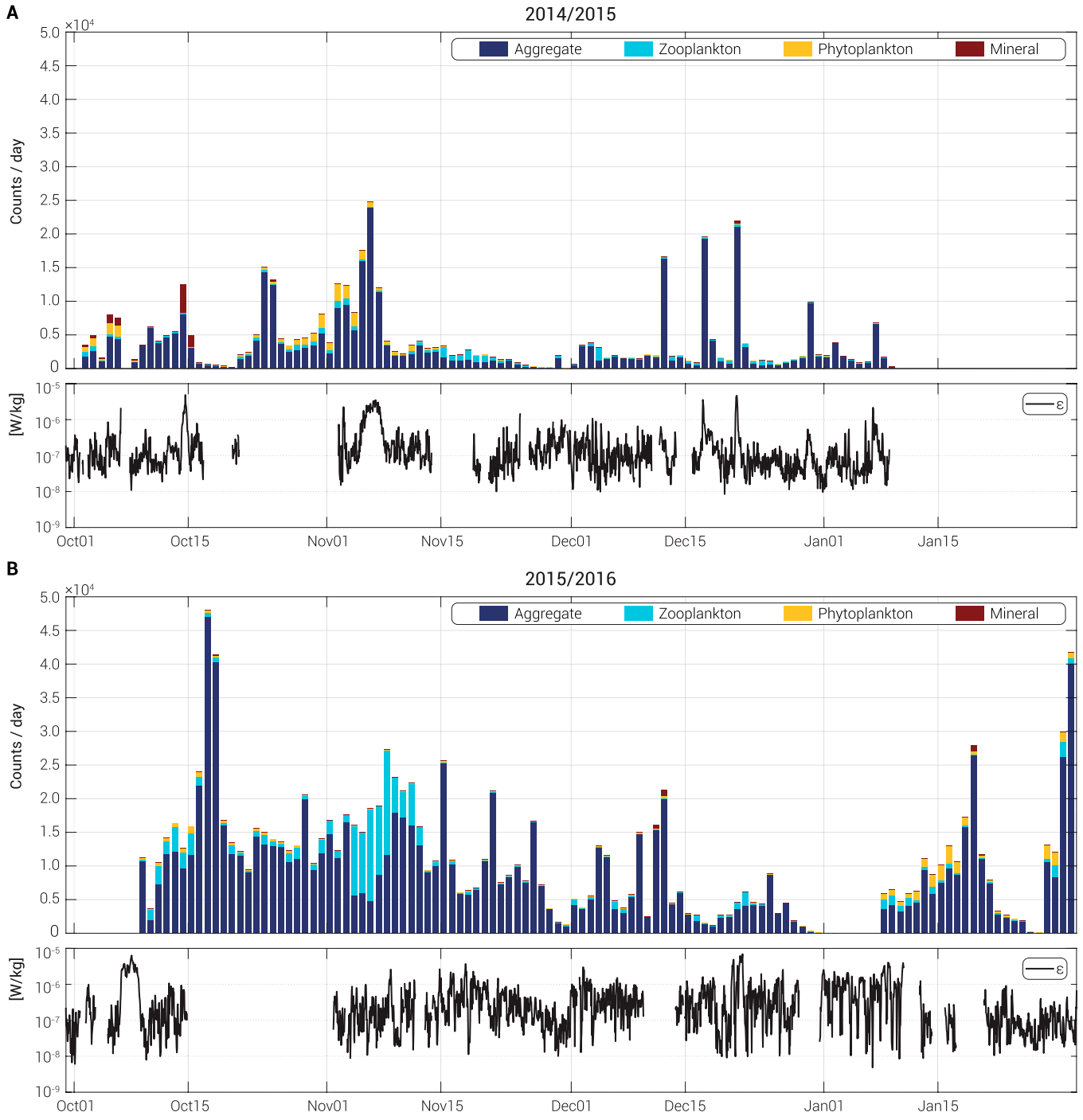

Fig. 6. Average daily abundance of aggregates, zooplankton, phytoplankton, and mineral particles (color bars) and the hourly rate of turbulent kinetic energy dissipation, ε, for TS1 (A) and (B) TS2. The law of the wall method was used to estimate ε, according to Tanaka et al. [21].

plankton and particle (aggregate) abundance and diversity respond rapidly to changes in oceanographic conditions.

Diversity estimates based on broad taxonomic categories reflect limitations of the CPICS imaging system, which lacks species-level resolution. Despite reduced taxonomic precision, it permits meaningful assessment of structural shifts in the plankton communities over time [60,61]. The inclusion of nonliving biogenic particles, such as fecal pellets and marine aggregates, enhances the ecological value of the diversity index. These particles, products of biological activity, influence microbial colonization, nutrient recycling, and vertical flux, offering a broader functional view of planktonic ecosystem dynamics [62,63].

The primary environmental difference between the 2 datasets was the presence of distinct water masses, as revealed by the TS diagram (Fig. 2) and confirmed by RDA (Fig. 10). TS1 (October 2014 to January 2015) was characterized by warmer, more saline waters, indicative of open-ocean conditions likely

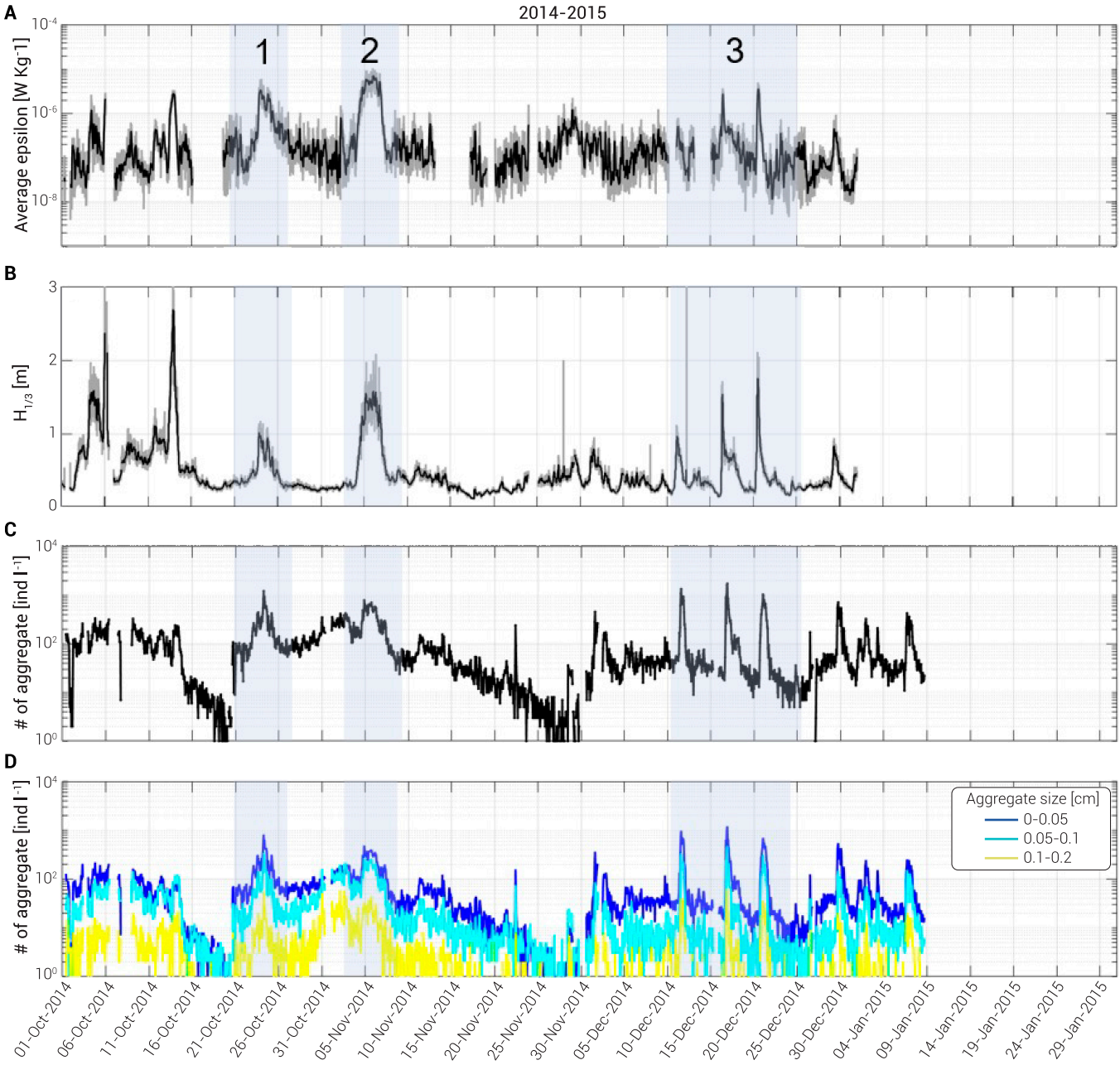

Fig. 7. Time series (hourly averages) of turbulent intensity (A), wave heights (B), number of aggregates (C), and the composition of aggregate size classes for TS1 (D). The shaded vertical areas represent the 3 major storm events, marked in sequential numbers in the upper panel.

influenced by the Kuroshio. In contrast, TS2 (October 2015 to January 2016) exhibited cooler, less saline waters typical of coastal environments, potentially originating from Tokyo Bay. TS2 also exhibited increased compact aggregates and smaller zooplankton, particularly copepods, and a decrease in the percentage of diatoms. These findings align with prior observations linking coastal copepod abundance to low-salinity waters, i.e., elevated plankton standing stocks, particularly coastal copepods, are associated with the intrusion of low-salinity waters in Kuroshio-influenced regions [58]. Such interannual variability is indicative of the dynamic exchange between oceanic (Kuroshio-dominated) and continental shelf waters in the region. Temporal changes in plankton assemblages observed at fixed stations often reflect seasonal variations or small-scale horizontal advection [59], emphasizing the need to account for both temporal and spatial factors when interpreting plankton community dynamics.

Short-term fluctuations in plankton diversity are closely linked to changes in turbulence levels. Wind-induced turbulence efficiently transports inorganic nutrients to shallow euphotic zones [60,61]. In combination with tidal currents, turbulence can promote sediment resuspension [46], as observed following the October 2014 typhoon and subsequent events. Although mechanisms driving eukaryotic plankton diversity in coastal waters remain underexplored, it is plausible that dynamic processes, such as wave action, tidal mixing, and salinity fluctuations, favor

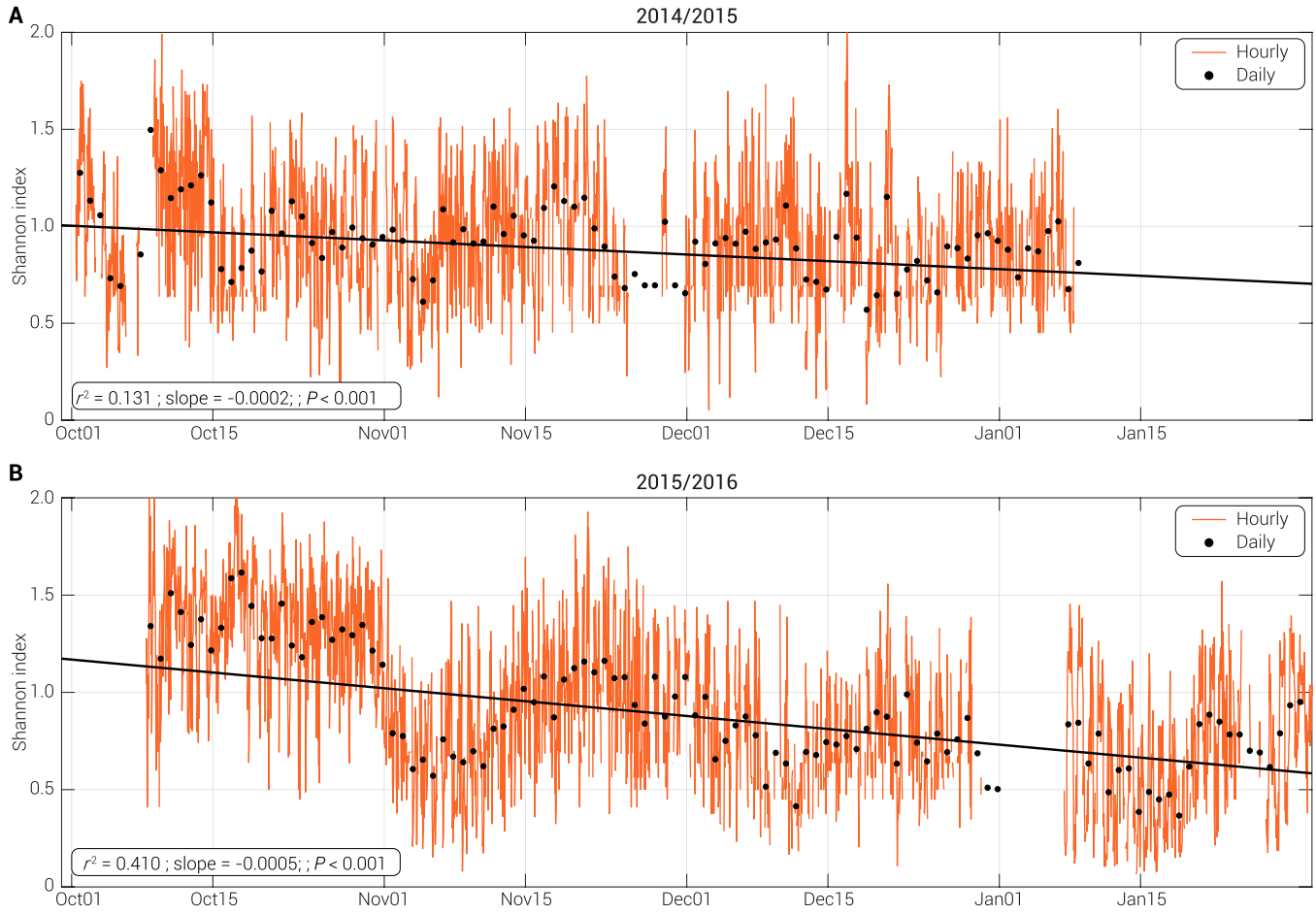

Fig. 8. Time series of the Shannon diversity index for (A) TS1, 2014/2015 and (B) TS2, 2015/2016.

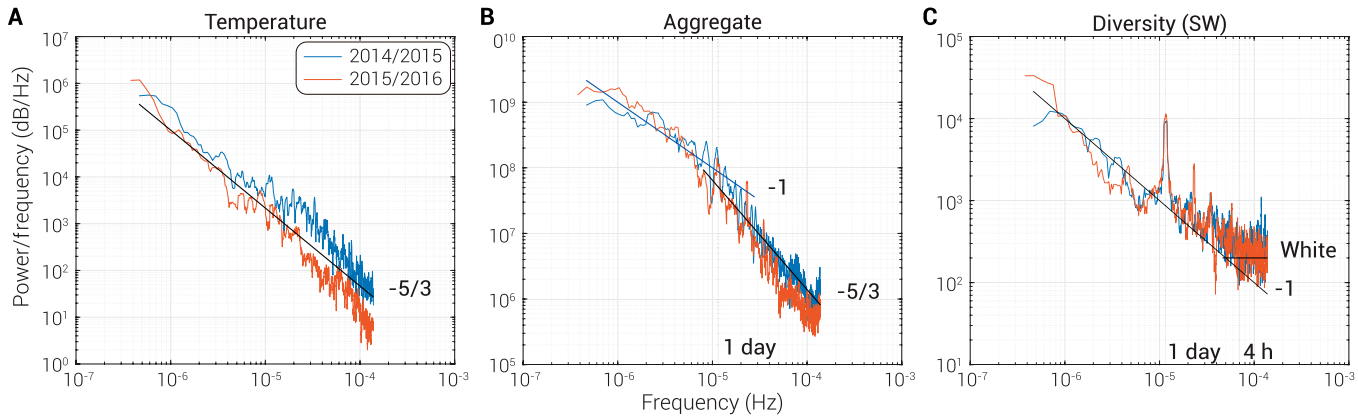

Fig. 9. Power spectrum density (PSD) for each time series interval. (A) Temperature. (B) Aggregate (hourly data). (C) Shannon diversity index (hourly data).

species adaptation to high environmental variability [62]. This adaptability likely results in reduced diversity compared with open-ocean environments. Increased turbulence, turbidity, and nutrient inputs in coastal waters are often associated with elevated phytoplankton and zooplankton biomasses [63].

The −5/3 slope recorded in the temperature time series for both observation periods is consistent with the turbulence theory, reflecting the presence of an inertial subrange and turbulent mixing within the upper water column [64]. For hourly aggregate abundance, PSD analysis indicated that short cycles (below daily timescales) were influenced by turbulence, whereas long-term fluctuations followed distinct nonlinear dynamics, exhibiting a 1/f slope characteristic of pink noise.

RDA analysis indicated a strong positive correlation between turbulent energy dissipation rate (ε) and aggregate abundance. The coincident temporal trends of wind speed and turbidity suggest that increases in particle abundance were dominated by the resuspension of aggregates from the bottom boundary layer.

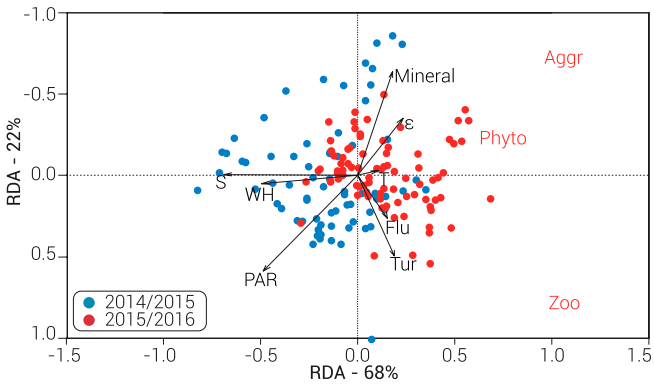

Fig. 10. Redundancy analysis (RDA) biplot of sampling period scores for environmental and biological variables. Blue and red dots represent data from TS1 and TS2, respectively. Arrows point in the direction of maximum variability explained by the respective environmental variable (T, temperature; S, salinity; PAR, photosynthetically active radiation; Flu, chlorophyll-a fluorescence; Tur, turbidity; ε, turbulent kinetic energy dissipation rate; Mineral, suspended mineral particles; WH, significant wave height). The biological variables are shown in red font (Phyto, phytoplankton; Zoo, zooplankton; Aggr, aggregates).

However, the formation of aggregates by particle collision due to elevated turbulence may have also contributed to the increase in aggregate abundance [5]. Furthermore, concurrent phytoplankton and aggregate maxima in late October and early November during TS1 suggest that nutrient input from sediment resuspension can promote phytoplankton growth, with the subsequent sinking of phytoplankton contributing to aggregate formation.

PSD analysis of the Shannon diversity index revealed a 1/f slope at low frequencies, indicating a self-organized system governed by nonlinear dynamics distinct from the turbulence spectrum. The observed 1-d periodicity in diversity aligns with the diel vertical migration (DVM) of zooplankton, which enhances surface diversity as deep-dwelling taxa ascend at night. These findings emphasize the importance of zooplankton behavior, particularly DVM, in shaping plankton and particle diversity, a factor often overlooked in DVM research [65].

High-frequency time series observations at the Japanese coastal site of Oshima demonstrated that plankton and particle abundance are strongly coupled with oceanographic properties. The observed alignment between low-salinity water intrusion and elevated plankton standing stocks highlights the interplay between oceanic and continental shelf waters, with variability at interannual scales. The correlations among turbulence, plankton diversity, and aggregate dynamics provide new insights into the ecological processes governing coastal marine ecosystems.

Acknowledgments

We extend our profound gratitude to the staff of the Tokyo Metropolitan Islands area Research and Development Center for Agriculture, Forestry, and Fisheries for their invaluable logistics support. The sustained operation of the OCEANS cable observatory was made possible through the dedicated efforts of K. Yamaguchi. We thank the anonymous reviewers for their helpful comments on this manuscript.

Funding: This work was supported by JST CREST grant number JPMJCR12A6.

Author contributions: H.Y. conceived this study. G.F., M. Takeuchi, M. Tanaka, and H.Y. conducted the experiment at the cabled observatory site. G.F., M. Takeuchi, M. Tanaka, and L.D. analyzed the data. All authors contributed to the interpretation of the results; H.Y., S.B.P., and R.L. wrote the first draft, and all authors contributed to the final manuscript.

Competing interests: The authors declare that they have no competing interests.

Data Availability

The raw data can be obtained from the following data archive system: https://dbarchive.biosciencedbc.jp/en/jedisystem-oceansdb/desc.html.

Supplementary Materials

Table S1

References

1. Sabine CL, Feely RA, Gruber N, Key RM, Lee K, Bullister JL, Wanninkhof R, Wong CSL, Wallace DWR, Tilbrook B, et al. The oceanic sink for anthropogenic CO2. *Science*. 2004;305(3682):367–371.
2. Tréguer P, Bowler C, Moriceau B, Dutkiewicz S, Gehlen M, Aumont O, Bittner L, Dugdale R, Finkel Z, Iudicone D, et al. Influence of diatom diversity on the ocean biological carbon pump. *Nat Geosci*. 2018;11(1):27–37.
3. Macías D, Rodríguez-Santana Á, Ramírez-Romero E, Bruno M, Pelegrí JL, Sangrà P, Aguiar-González B, García CM, et al. Turbulence as a driver for vertical plankton distribution in the subsurface upper ocean. *Sci Mar*. 2013;77(4):541–549.
4. Durham WM, Climent E, Barry M, de Lillo F, Boffetta G, Cencini M, Stocker R. Turbulence drives microscale patches of motile phytoplankton. *Nat Commun*. 2013;4(1):2148.
5. Takeuchi M, Doubell MJ, Jackson GA, Yukawa M, Sagara Y, Yamazaki H. Turbulence mediates marine aggregate formation and destruction in the upper ocean. *Sci Rep*. 2019;9(1):16280.
6. Takeuchi M, Giering S, Yamazaki H. Size distribution of aggregates across different aquatic systems around Japan shows that stronger aggregates are formed under turbulence. *Limnol Oceanogr*. 2024;69(11):2580–2595.
7. Iversen MH. Carbon export in the ocean: A biologist's perspective. *Annu Rev Mar Sci*. 2023;15(1):357–381.
8. Behrenfeld MJ, O'Malley RT, Siegel DA, McClain CR, Sarmiento JL, Feldman GC, Milligan AJ, Falkowski PG, Letelier RM, Boss ES. Climate-driven trends in contemporary ocean productivity. *Nature*. 2006;444(7120):752–755.
9. Munk W, Wunsch C. Abyssal recipes II: Energetics of tidal and wind mixing. *Deep Sea Res*. 1998;45(12):1977–2010.
10. Kerry CG, Powell BS, Carter GS. The impact of subtidal circulation on internal tide generation and propagation in the Philippine Sea. *J Phys Oceanogr*. 2014;44(5):1386–1405.
11. Whalen CB, MacKinnon JA, Talley LD. Large-scale impacts of the mesoscale environment on mixing from wind-driven internal waves. *Nat Geosci*. 2018;11(11):842–847.
12. Richards KJ, Kashino Y, Natarov A, Firing E. Mixing in the western equatorial Pacific and its modulation by ENSO. *Geophys Res Lett*. 2012;39(2).
13. Sasaki W, Richards KJ, Luo J-J. Impact of vertical mixing induced by small vertical scale structures above and within the equatorial thermocline on the tropical Pacific in a CGCM. *Clim Dyn*. 2013;41(2):443–453.

14. Franks PJS, Inman BG, MacKinnon JA, Alford MH, Waterhouse AF. Oceanic turbulence from a planktonic perspective. *Limnol Oceanogr*. 2022;67(2):348–363.
15. Tozzi S, Schofield O, Falkowski P. Historical climate change and ocean turbulence as selective agents for two key phytoplankton functional groups. *Mar Ecol Prog Ser*. 2004;274:123–132.
16. Barton AD, Ward BA, Williams RG, Follows MJ. The impact of fine-scale turbulence on phytoplankton community structure. *Limnol Oceanogr Fluids Environ*. 2014;4(1):34–49.
17. Estrada M, Berdalet E. Phytoplankton in a turbulent world. *Sci Mar*. 1997;61:125–140.
18. Rothschild BJ, Osborn TR. Small-scale turbulence and plankton contact rates. *J Plankton Res*. 1988;10(3):465–474.
19. Haury LR, Yamazaki H, Itsweire EC. Effects of turbulent shear flow on zooplankton distribution. *Deep Sea Res.* 1990;37(3):447–461.
20. Smyth TJ, Allen I, Atkinson A, Bruun JT, Harmer RA, Pingree RD, Widdicombe CE, Somerfield PJ. Ocean net heat flux influences seasonal to interannual patterns of plankton abundance. *PLOS ONE*. 2014;9(2):Article e98709.
21. Tanaka M, Genin A, Endo Y, Ivey GN, Yamazaki H. The potential role of turbulence in modulating the migration of demersal zooplankton. *Limnol Oceanogr*. 2020;66(3):855–864.
22. Eloire D, Somerfield PJ, Conway DVP, Halsband-Lenk C, Harris R, Bonnet D. Temporal variability and community composition of zooplankton at station L4 in the Western Channel: 20 years of sampling. *J Plankton Res*. 2010;32(5):657–679.
23. Romano F, Symiakaki K, Pitta P. Temporal variability of planktonic ciliates in a coastal oligotrophic environment: Mixotrophy, size classes and vertical distribution. *Front Mar Sci*. 2021;8:Article 641589.
24. Widdicombe CE, Eloire D, Harbour D, Harris RP, Somerfield PJ. Long-term phytoplankton community dynamics in the Western English Channel. *J Plankton Res*. 2010;32(5):643–655.
25. Vantrepotte V, Mélin F. Temporal variability of 10-year global SeaWiFS time-series of phytoplankton chlorophyll a concentration. *ICES J Mar Sci*. 2009;66(7):1547–1556.
26. Strickland JDH. A comparison of profiles of nutrient and chlorophyll concentrations taken from discrete depths and by continuous recording. *Limnol Oceanogr*. 1968;13(2):388–391.
27. Mandal S, Locke C, Tanaka M, Yamazaki H. Observations and models of highly intermittent phytoplankton distributions. *PLOS ONE*. 2014;9(5):Article e94797.
28. Doubell MJ, Yamazaki H, Li H, Kokubu Y. An advanced laser-based fluorescence microstructure profiler (TurboMAP-L) for measuring bio-physical coupling in aquatic systems. *J Plankton Res*. 2009;31(12):1441–1452.
29. Dahms H-U, Hwang J-S. Perspectives of underwater optics in biological oceanography and plankton ecology studies. *J Mar Sci Technol*. 2010;18(1):14.
30. Jaffe JS. Underwater optical imaging: The past, the present, and the prospects. *IEEE J Ocean Eng*. 2014;40(3):683–700.
31. Kiko R, Lopes RM, Soviadan YD, Stemmann L. Towards a distributed and operational pelagic imaging network. *Ocean Coast Res*. 2023;71:Article e23058.
32. Talapatra S, Hong J, McFarland M, Nayak AR, Zhang C, Katz J, Sullivan J, Twardowski M, Rines J, Donaghay P. Characterization of biophysical interactions in the water column using in situ digital holography. *Mar Ecol Prog Ser*. 2013;473:29–51.
33. Ohman MD, Davis RE, Sherman JT, Grindley KR, Whitmore BM, Nickels CF, Ellen JS. Zooglider: An autonomous vehicle for optical and acoustic sensing of zooplankton. *Limnol Oceanogr Methods*. 2019;17(1):69–86.
34. Nayak AR, Malkiel E, McFarland MN, Twardowski MS, Sullivan JM. A review of holography in the aquatic sciences: In situ characterization of particles, plankton, and small scale biophysical interactions. *Front Mar Sci*. 2021;7:Article 572147.
35. Giering SLC, Cavan EL, Basedow SL, Briggs N, Burd AB, Darroch LJ, Guidi L, Irisson J-O, Iversen MH, Kiko R, et al. Sinking organic particles in the ocean—Flux estimates from in situ optical devices. *Front Mar Sci*. 2020;6:834.
36. Olson RJ, Sosik HM. A submersible imaging-in-flow instrument to analyze nano-and microplankton: Imaging FlowCytobot. *Limnol Oceanogr Methods*. 2007;5(6):195–203.
37. Orenstein EC, Ratelle D, Briseño-Avena C, Carter ML, Franks PJS, Jaffe JS, Roberts PLD. The Scripps Plankton Camera system: A framework and platform for in situ microscopy. *Limnol Oceanogr Methods*. 2020;18(11):681–695.
38. Boss E, Waite AM, Karstensen J, Trull T, Muller-Karger F, Sosik HM, Uitz J, Acinas SG, Fennel K, Berman-Frank I, et al. Recommendations for plankton measurements on OceanSITES moorings with relevance to other observing sites. *Front Mar Sci*. 2022;9:Article 929436.
39. Campbell L, Henrichs DW, Olson RJ, Sosik HM. Continuous automated imaging-in-flow cytometry for detection and early warning of Karenia brevis blooms in the Gulf of Mexico. *Environ Sci Pollut Res*. 2013;20(10):6896–6902.
40. Catlett D, Peacock EE, Crockford ET, Futrelle J, Batchelder S, Stevens BLF, Gast RJ, Zhang WG, Sosik HM. Temperature dependence of parasitoid infection and abundance of a diatom revealed by automated imaging and classification. *Proc Natl Acad Sci USA*. 2023;120(28):Article e2303356120.
41. Yamazaki H, Gallager S, Tanaka M, Yamaguchi K. A cabled observatory system for integrated long term, high-frequency biological, chemical, physical measurement for understanding planktonic ecosystem. *IEEE Technol Ocean*. 2016;2016:429–434.
42. Tanaka M, Genin A, Lopes RM, Stricker JR, Yamazaki H. Biased measurements by stationary turbidity-fluorescence instruments due to phototactic zooplankton behavior. *Limnol Oceanogr Method*. 2019;17(9):505–513.
43. Masunaga E, Fringer O, Kitade Y, Yamazaki H, Gallager S. Dynamics and energetics of trapped diurnal internal Kelvin waves around a mid-latitude island. *J Phys Oceanogr*. 2017;47(10):2479–2498.
44. Grossmann MM, Gallager SM, Mitarai S. Continuous monitoring of near-bottom mesoplankton communities in the East China Sea during a series of typhoons. *J Oceanogr*. 2015;71(1):115–124.
45. Penninck SB, Lopes RM, Lima JF, McManus MA. Thin layers in the coastal zone of Ubatuba, Brazil: Mechanisms of formation and dissipation. *Limnol Oceanogr*. 2021;66(2):558–574.
46. Penninck SB, Lopes RM. Short-term variability in plankton abundance on the inner shelf off Ubatuba. *Brazil J Plankton Res*. 2023;45(3):485–508.
47. Dougherty ER, Lotufo RA. *Hands-on morphological image processing*. Bellingham (WA): SPIE Optical Engineering Press; 2003.
48. Gonzalez RC. *Digital image processing*. 2nd ed. Delhi (India): Prentice-Hall of India; 2002.

49. Ahonen T, Matas J, He C, Pietikäinen M. Rotation invariant image description with local binary pattern histogram Fourier features. In: Salberg AB, Hardeberg JY, Jenssen R, editors. *Image analysis. SCIA 2009. Lecture Notes in Computer Science, vol 5575*. Berlin, Heidelberg: Springer; 2009. p. 61–70.
50. Ojala T, Pietikäinen M, Mäenpää T. Gray scale and rotation invariant texture classification with local binary patterns. *In Pract*. 2000;1842:404–420.
51. Haralick R, Shanmugan K, Dinstein I. Textural features for image classification. In: *IEEE Transactions on Systems, Man and Cybernetics*. Piscataway (NJ): IEEE; 1973. Vol. 3, p. 610–621.
52. Gorsky G, Ohman MD, Picheral M, Gasparini S, Stemmann L, Romagnan J-B, Cawood A, Pesant S, García-Comas C, Prejger F. Digital zooplankton image analysis using the ZooScan integrated system. *J Plankton Res*. 2010;32(3):285–303.
53. Hirata NST, Fernandez M, Lopes RM. Plankton image classification based on multiple segmentations. In: *Proceedings of the 2nd Workshop on Computer Vision for Analysis of Underwater Imagery, CVAUI 2016 - In Conjunction with International Conference on Pattern Recognition, ICPR 2016*. Los Alamitos (CA): IEEE; 2017.
54. Rodrigues FCM, Hirata NST, Abello AA, de La Cruz LT, Lopes RM, Hirata R. Evaluation of transfer learning scenarios in plankton image classification. In: *VISIGRAPP (5: VISAPP)*. Setúbal (Portugal): SciTePress; 2018. p. 359–366.
55. Schmid MS, Aubry C, Grigor J, Fortier L. The LOKI underwater imaging system and an automatic identification model for the detection of zooplankton taxa in the Arctic Ocean. *Methods Oceanogr*. 2016;15-16:129–160.
56. Breiman L. Random forests. *Mach Learn*. 2001;45(1):5–32.
57. Shannon CE. A mathematical theory of communication. *Bell Syst Tech J*. 1948;27(4):379–423.
58. Oksanen J, Simpson G, Blanchet F, Kindt R, Legendre P, Minchin P, O'Hara R, Solymos P, Stevens M, Szoecs E, et al. vegan: Community Ecology Package. R package version 2.8-0. 2025. https://vegandevs.github.io/vegan/
59. Tennekes H, Lumley JL. *A first course in turbulence*. 2nd ed. Cambridge (MA): MIT Press; 1982.
60. Lombard F, Boss E, Waite AM, Vogt M, Uitz J, Stemmann L, Sosik HM, Schulz J, Romagnan J-B, Picheral M, et al. Globally consistent quantitative observations of planktonic ecosystems. *Front Mar Sci*. 2019;6.
61. Irisson J, Ayata S, Lindsay DJ, Karp-Boss L, Stemmann L. Machine learning for the study of plankton and marine snow from images. *Annu Rev Mar Sci*. 2022;14:277–301.
62. Alldredge AL, Silver MW. Characteristics, dynamics and significance of marine snow. *Prog Oceanogr*. 1988;20(1):41–82.
63. Turner JT. Zooplankton fecal pellets, marine snow, phytodetritus and the ocean's biological pump. *Prog Oceanogr*. 2015;130:205–248.
64. Kobari T, Makihara W, Kawafuchi T, Sato K, Kume G. Geographic variability in taxonomic composition, standing stock, and productivity of the mesozooplankton community around the Kuroshio current in the East China Sea. *Fish Oceanogr*. 2018;27(4):336–350.
65. Lévy M, Jahn O, Dutkiewicz S, Follows MJ, d'Ovidio F. The dynamical landscape of marine phytoplankton diversity. *J R Soc Interface*. 2015;12(111):Article 20150481.

Ocean - Land - Atmosphere Research
A SCIENCE PARTNER JOURNAL

High-Frequency Observations of Plankton and Particle Abundance from a Cabled Observatory Off Japan

Hidekatsu Yamazaki, Silvana B. Penninck, Gabriel Freitas, Leandro T. De-La-Cruz, Marika Takeuchi, Mamoru Tanaka, and Rubens M. Lopes

Citation: Yamazaki H, Penninck S, Freitas G, De-La-Cruz L, Takeuchi M, Tanaka M, Lopes R. High-Frequency Observations of Plankton and Particle Abundance from a Cabled Observatory Off Japan. *Ocean-Land-Atmos Res*. 2026;**5**:0132. DOI: 10.34133/olar.0132

In August 2014, a cabled observatory was deployed off Oshima Island, south of Tokyo, Japan, and operated until September 2018, yielding a 4-year dataset of oceanographic properties and plankton abundance at a fixed location. This study highlights the variability of key physical and biological parameters observed during 2 distinct periods of this time series. Data were collected using a suite of instruments such as thermistor chains, acoustic Doppler velocimeter (ADV), acoustic Doppler current profiler (ADCP), conductivity, temperature, depth (CTD), turbidity and fluorescence sensor, photosynthetically active radiation (PAR) sensor, wave height gauge, and CPICS (a plankton imaging system). Based on these observations, the kinetic energy dissipation rate was estimated over time and its correlation with plankton abundance, aggregate abundance, and plankton diversity was examined. The results demonstrated that temperature fluctuations followed a #5/3 power-law spectrum across the observed frequency range, consistent with turbulence theory. Plankton diversity, measured using the Shannon index, exhibited a power-law spectrum with a slope of #1 (*f*#1) for harmonic components exceeding 4 h in duration, characterized by a daily peak corresponding to zooplankton diel vertical migration. Long-term measurements of turbulence remain scarce but are crucial for understanding seasonal to interannual variability in plankton and particle dynamics. These findings underscore the importance of ocean mixing in regulating size distribution and abundance, offering insights into the interplay between physical and biological processes in coastal ecosystems.
Image

Ocean-Land-Atmosphere Research (ISSN 2771-0378) is published by the American Association for the Advancement of Science. 1200 New York Avenue NW, Washington, DC 20005.